JOURNAL OF SOLID STATE CHEMISTRY 120, 112–120 (1995)

Syntheses, Crystal Structures, and Properties of New Layered Tungsten(VI)-Containing Materials Based on the Hexagonal-WO_3 Structure: $M_2(WO_3)_3SeO_3$ (M = NH_4, Rb, Cs)

William T. A. Harrison, Laurie L. Dussack, Thomas Vogt,* and Allan J. Jacobson

*Department of Chemistry, University of Houston, Houston, Texas 77204-5641; and *Physics Department, Brookhaven National Laboratory, Upton, New York 11973*

Received May 5, 1995; in revised form July 18, 1995; accepted July 26, 1995

The hydrothermal syntheses and crystal structures of $(NH_4)_2(WO_3)_3SeO_3$ and $Cs_2(WO_3)_3SeO_3$, two new noncentrosymmetric, layered tungsten(VI)-containing phases are reported. Infrared, Raman, and thermogravimetric data are also presented. $(NH_4)_2(WO_3)_3SeO_3$ and $Cs_2(WO_3)_3SeO_3$ are isostructural phases built up from hexagonal-tungsten-oxide-like, anionic layers of vertex-sharing WO_6 octahedra, capped on one side by Se atoms (as selenite groups). Interlayer NH_4^+ or Cs^+ cations provide charge balance. The full H-bonding scheme in $(NH_4)_2(WO_3)_3SeO_3$ has been elucidated from Rietveld refinement against neutron powder diffraction data. The WO_6 octahedra display a 3 short + 3 long W—O bond-distance distribution within the WO_6 unit in both these phases. $(NH_4)_2(WO_3)_3SeO_3$ and $Cs_2(WO_3)_3SeO_3$ are isostructural with their molybdenum(VI)-containing analogues $(NH_4)_2(MoO_3)_3SeO_3$ and $Cs_2(MoO_3)_3SeO_3$. Crystal data: $(NH_4)_2(WO_3)_3SeO_3$, M_r = 858.58, hexagonal, space group $P6_3$ (No. 173), a = 7.2291(2) Å, c = 12.1486(3) Å, V = 549.82(3) Å^3, Z = 2, R_p = 1.81%, and R_{wp} = 2.29% (2938 neutron powder data). $Cs_2(WO_3)_3SeO_3$, M_r = 1088.31, hexagonal, space group $P6_3$ (no. 173), a = 7.2615(2) Å, c = 12.5426(3) Å, V = 572.75(3) Å^3, Z = 2, R_p = 4.84%, and R_{wp} = 5.98% (2588 neutron powder data). © 1995 Academic Press, Inc.

INTRODUCTION

We have recently reported the syntheses and structures of several new layered materials based on the hexagonal-tungsten-oxide (HTO) motif of corner-sharing octahedra (1–3). This in-layer connectivity (Fig. 1) results in a hexagonal array of three- and six-rings of octahedra. (In hex-WO_3 itself (4), the WO_3 layers are fused together via apical W—O—W′ bonds, and a three-dimensional W/O topology results).

$NH_4(VO_2)_3(SeO_3)_2$ (1) contains vanadium (V) as the octahedral cation, and both sides of the infinite vanadium/oxygen layers are capped by selenium atoms (as pyramidal $[SeO_3]^{2-}$ selenite groups). $K(VO_2)_3(SeO_3)_2$ (5) has the same structure as $NH_4(VO_2)_3(SeO_3)_2$. The isostructural $(NH_4)_2(MoO_3)_3SeO_3$ and $Cs_2(MoO_3)_3SeO_3$ (2) contain similar vertex-linked MoO_6 layers (Mo^{VI}), but are only capped by Se^{IV} atoms ($[SeO_3]^{2-}$ selenite groups) on one side of the molybdenum/oxygen sheets. $Cs_2(MoO_3)_3PO_3CH_3$ and $Rb_2(MoO_3)_3PO_3CH_3$ (3) are also built up from infinite molybdenum/oxygen sheets, but in this case, the capping group is PCH_3 (as part of a $[O_3P—CH_3]^{2-}$ methylphosphonate group). The alkali-metal/ammonium cations provide interlayer charge-balancing in all these phases.

In this paper we report the syntheses, structures, and some properties of $(NH_4)_2(WO_3)_3SeO_3$ and $Cs_2(WO_3)_3SeO_3$, two tungsten(VI)-containing analogues of the $M_2(MoO_3)_3SeO_3$ materials. $Rb_2(WO_3)_3SeO_3$ has also been prepared.

SYNTHESIS AND INITIAL CHARACTERIZATION

$(NH_4)_2(WO_3)_3SeO_3$ was prepared from the hydrothermal reaction of 0.4 g $(NH_4)_{10}W_{12}O_{41}$ (1.58 mmole W), 0.407 g H_2SeO_3 (3.16 mmole Se), 0.098 g NH_4Cl (1.84 mmole NH_4), and 10 ml water (NH_4 : W : Se ratio = 2 : 1 : 2). Heating these reactants to 200°C for 7 days in a sealed, Teflon-lined, 23-ml capacity Parr hydrothermal reaction vessel resulted in many tiny hexagonal crystals (82% yield based on W, final pH 2.2) after product recovery. These crystals were too small for single crystal X-ray measurements, and they were ground to a white, microcrystalline powder for powder diffraction studies. The use of higher concentrations of starting components resulted in higher yields of $(NH_4)_2(WO_3)_3SeO_3$, but lower crystallinity (as gauged from powder X-ray data). Reactions which omitted the ammonium chloride resulted in lower yields of $(NH_4)_2(WO_3)_3SeO_3$ and WO_3 impurity (by powder X-ray measurements).

$Cs_2(WO_3)_3SeO_3$ was prepared from a mixture of 0.6 g WO_3 (2.6 mmole W), 0.847 g Cs_2CO_3 (5.2 mmole Cs),

0022-4596/95 $12.00

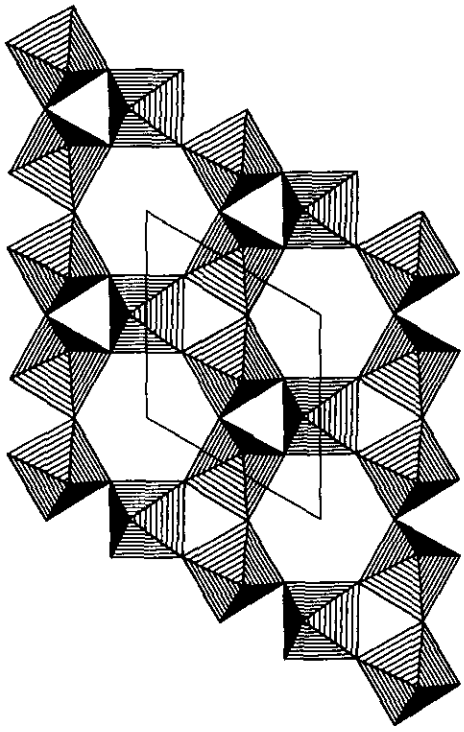

FIG. 1. Polyhedral plot down [001] of one layer of a hexagonal tungsten-oxide-type phase, showing the resulting three- and six-rings of octahedra. The apical connectivity of these layers determines the dimensionality of the structure (see text).

0.667 g H_2SeO_3 (5.2 mmole Se), and 10 ml deionized water (Cs : W : Se molar ratio 2 : 1 : 2). These reactants were sealed in a Teflon-lined 23-ml capacity Parr hydrothermal reaction vessel, and heated to 210°C for 12 days, followed by slow cooling to ambient over 24 hr. White microcrystalline powder was recovered by vacuum filtration (98% yield based on W; pH of filtrate 3.3).

$Rb_2(WO_3)_3SeO_3$ was hydrothermally prepared from 0.6 g WO_3 (2.6 mmol W), 0.577 g SeO_2 (5.2 mmol Se), 0.600 g Rb_2CO_3 (5.2 mmol Rb), and 10 ml H_2O. These reactants were heated to 210°C for 10 days in a Parr hydrothermal bomb. Product recovery by vacuum filtration (filtrate pH 3.4) resulted in a white microcrystalline powder (86% yield).

X-ray powder data for thoroughly ground samples of $(NH_4)_2(WO_3)_3SeO_3$ and $Cs_2(WO_3)_3SeO_3$ were recorded on a Scintag XDS 2000 automated powder diffractometer [Cu$K\alpha$ radiation, $\bar{\lambda}$ = 1.54178 Å, T = 25(2)°C]. $(NH_4)_2(WO_3)_3SeO_3$ and $Cs_2(WO_3)_3SeO_3$ yielded similar patterns which could be indexed on hexagonal unit cells [for $(NH_4)_2(WO_3)_3SeO_3$, a = 7.2282(2) Å, c = 12.1470(5) Å, and V = 549.6 Å^3; for $Cs_2(WO_3)_3SeO_3$, a = 7.251(2) Å, c = 12.527(2) Å, and V = 570.4 Å^3]. These primitive hexagonal cells (absence condition 000l, $l = 2n$) suggested that $(NH_4)_2(WO_3)_3SeO_3$ and $Cs_2(WO_3)_3SeO_3$ were isostructural with the molybdenum-containing materials $(NH_4)_2(MoO_3)_3SeO_3$ and $Cs_2(MoO_3)_3SeO_3$ (2), as was found to be the case (*vide infra*). The $Rb_2(WO_3)_3SeO_3$ powder gave a similar hexagonal pattern (a = 7.2834(4) Å, c = 11.965(1) Å, and V = 549.7 Å^3), but lines due to triclinic WO_3 were also present.

Thermogravimetric analysis data for $(NH_4)_2(WO_3)_3SeO_3$ and $Cs_2(WO_3)_3SeO_3$ were collected on a DuPont 9900 analyzer under flowing O_2 or N_2 gas (see below). The post-TGA residues were analyzed by powder X-ray diffraction.

Infrared spectra (KBr pellet method) for the title compounds were recorded between 400 and 4000 cm^{-1} on a Galaxy FTIR 5000 series spectrometer. Raman data (KCl pellet method) for $Cs_2(WO_3)_3SeO_3$ were obtained using a coherent K-2 Kr+ ion laser excited at 406.7 nm. Counts were accumulated at 1-s intervals for every wavenumber over the range 100–1700 cm^{-1} (Spex 1403 double monochromator/Hamamatsu 928 photomultiplier detection system).

CRYSTAL STRUCTURE DETERMINATION

Since we have been unable to grow suitably sized single crystals for X-ray diffraction measurements of these materials, we proceeded to refine their crystal structures by the Rietveld method. In order to maximize the refinement precision of the lighter atoms, constant-wavelength neutron powder data were collected for both $(NH_4)_2(WO_3)_3SeO_3$ and $Cs_2(WO_3)_3SeO_3$. Large samples of the NH_4 and Cs compounds were obtained by multiple repetitions of the synthesis procedures given above.

For each material, ~10-g quantities of sample were loaded and sealed into cylindrical vanadium sample cans. Room temperature, high-resolution powder data were collected on the HRNPD diffractometer at the High Flux Beam Reactor (HFBR), Brookhaven National Laboratory. Collection times of 12 hr for each sample resulted in satisfactory counting statistics ($5° < 2\theta < 165°$; step size = 0.05°; λ = 1.8857 Å). A characteristic, large incoherent background signal was observed for the $(NH_4)_2(WO_3)_3SeO_3$ sample, due to its proton content. However, previous experience has indicated that successful structure refinement, including location of H atoms, may be carried out on such patterns (6, 7).

The $(NH_4)_2(WO_3)_3SeO_3$ and $Cs_2(WO_3)_3SeO_3$ refinements were carried out using the program GSAS (8). Initial models, in space group $P6_3$ (No. 173), were based on the $(NH_4)_2(MoO_3)_3SeO_3$ and $Cs_2(MoO_3)_3SeO_3$ structures, respectively, with W substituting for Mo in each case. Starting cell parameters were taken from the powder X-ray measurements noted above. Coherent scattering lengths ($\times 10^{-10}$ cm) of b(N) = 0.930, b(H) = −0.374, b(Cs) = 0.542, b(W) = 0.477, b(Se) = 0.797, and b(O) = 0.581

TABLE 1
Crystallographic Parameters

	$(NH_4)_2(WO_3)_3SeO_3$	$Cs_2(WO_3)_3SeO_3$
Emp. formula	$W_3Se_1N_2O_{12}H_8$	$Cs_2W_3Se_1O_{12}$
Formula wt.	858.58	1088.31
Form	White powder	White powder
Crystal system	Hexagonal	Hexagonal
Space group	$P6_3$ (No. 173)	$P6_3$ (No. 173)
a (Å)	7.2291(2)	7.2615(2)
c (Å)	12.1486(3)	12.5426(3)
V (Å^3)	549.82(3)	572.75(3)
Z	2	2
ρ_{calc} (g/cm^3)	5.18	6.31
Radiation	Neutrons	Neutrons
λ (Å)	1.8857	1.8857
T (°C)	25(2)	25(2)
Powder data	2938	2588
Parameters	64	45
R_p[a] (%)	1.81	4.84
R_{wp}[b] (%)	2.29	5.98
χ^2	4.66	2.63

[a] $R_p = 100 \times \Sigma |y_o - \mathbf{C}y_c| / \Sigma |y_o|$.
[b] $R_{wp} = 100 \times [\Sigma w(y_o - \mathbf{C}y_c)^2 / \Sigma w y_o^2]^{1/2}$, where $\mathbf{C}$ is a scale factor.

were assumed. The refinements proceeded in typical fashion, with profile (scale factor, detector zero-point correction, polynomial background descriptors, peak shape parameters) and atomic positional and thermal parameters added to the model as additional variables as the refinement converged. Data with $2\theta < 20°$ were excluded from the $Cs_2(WO_3)_3SeO_3$ refinement due to gross peak asymmetry at low angles. In the latter stages of the $(NH_4)_2(WO_3)_3SeO_3$ refinement, the four crystallographic proton sites (*vide infra*) were located from Fourier difference maps and were added to the refinement as H atoms. For both phases, a simple Gaussian peak shape model was found to be inadequate, and a significantly better fit was obtained by using a pseudo-Voigt Gaussian/Lorentzian model. The $Cs_2(WO_3)_3SeO_3$ data showed anisotropic, *hkl*-dependent peak broadening, with the *hk*0 peaks significantly sharper than the 00*l* and *hkl* lines. Modeling this effect (8, 9), which might be due to stacking faults in the *z* direction, significantly improved the profile fit. At the conclusions of the refinements, convergence was achieved, and difference Fourier maps revealed no scattering maxima/minima which could be modeled as additional atomic sites.

Crystal and experimental data for these refinements are listed in Table 1. Final observed, calculated, and difference profile plots for $(NH_4)_2(WO_3)_3SeO_3$ and $Cs_2(WO_3)_3SeO_3$ are given in Figs. 2 and 3, respectively.

RESULTS

$(NH_4)_2(WO_3)_3SeO_3$. Final atomic positional and thermal parameters for $(NH_4)_2(WO_3)_3SeO_3$ are listed in Table 2, with selected bond distance/angle data in Table 3. $(NH_4)_2(WO_3)_3SeO_3$ is a new phase consisting of layers of vertex-sharing WO_6 and SeO_3 units, which are fused together by W—O—W and W—O—Se bonds. Ammonium cations provide interlayer charge balancing. The crystal structure of $(NH_4)_2(WO_3)_3SeO_3$ is illustrated in Figs. 4 and 5.

The tungsten atom in $(NH_4)_2(WO_3)_3SeO_3$ (W site symmetry 1) occupies a distorted octahedron, with a short "oxo" W=O(2) bond [d = 1.790(9) Å] not joined to any other atoms (except H bonds), a W(1)—O(4)—Se(1) link *trans* to this bond, and four W(1)—O—W(1)′ bonds via O(1) or O(3). The WO_6 octahedron in $(NH_4)_2(WO_3)_3SeO_3$ is significantly distorted from regular geometry—the W atom is displaced by 0.20 Å from the geometrical center of its O atom neighbors, which form a fairly regular octahedron (minimum O ··· O separation for *cis* O—W—O bonds is 2.65 Å, maximum is 2.73 Å). This distortion may be viewed as a local displacement of the W atom toward an octahedral face, resulting in three short (d < 1.85 Å) W—O bonds, each of which is *trans* to a long W—O (d > 1.99 Å) link. This WO_6 coordination is discussed below. A Brese–O'Keeffe bond valence sum (BVS) calculation (10) for W yields a value of 6.14, compared to the expected value of 6.00 for W^{VI}. The three short W—O bonds have BVS values in the range 0.63–0.82, whereas the three long W—O bonds have BVSs of 1.23–1.43.

The selenium atom (site symmetry 3) in $(NH_4)_2(WO_3)_3SeO_3$ shows typical pyramidal coordination, characteristic of the $[SeO_3]^{2-}$ selenite group (11) and makes three equivalent Se(1)—O(4)—W(1) bonds, each to a different W atom. Of the four distinct oxygen atoms, one, O(2), bonds only to W, two [O(1) and O(3)] bridge pairs of tungsten atoms, and one, O(4) links W and Se.

The two distinct ammonium cations in $(NH_4)_2(WO_3)_3SeO_3$ both have threefold symmetry, about an N—H bond aligned along the polar *z* axis. The location of the protons in the neutron diffraction experiment allows the H-bonding scheme to be elucidated in this phase: Three out of four hydrogen atoms make longish H bonds to nearby oxygen atom species (Table 3). N(1) is bonded to 3 × H(1) and H(3): Three N(1)—H(1) ··· O(4) H bonds form links with the oxygen atom bridging W and Se. In effect, the nitrogen atom of the $N(1)H_4$ group caps the W/O three rings not capped by the selenium atom. Conversely, H(3) makes no H-bonding connections, and the N(1)—H(3) bond points toward a six-ring opening in the adjacent $[(WO_3)_3SeO_3]^{2-}$ sheet. The equivalent isotropic thermal factor of H(3), the only H atom not involved in H bonding, is significantly larger than those of the other three H atoms. N(2) is bonded to 3 × H(2) and H(4). Three N(2)—H(2) ··· O(3) bonds are formed: The O(3) atoms form part of the six-ring in the hex-WO_3-type W/O sheets. A trifurcated N(2)—H(4) ··· [3 × O(2)] linkage is also formed by the

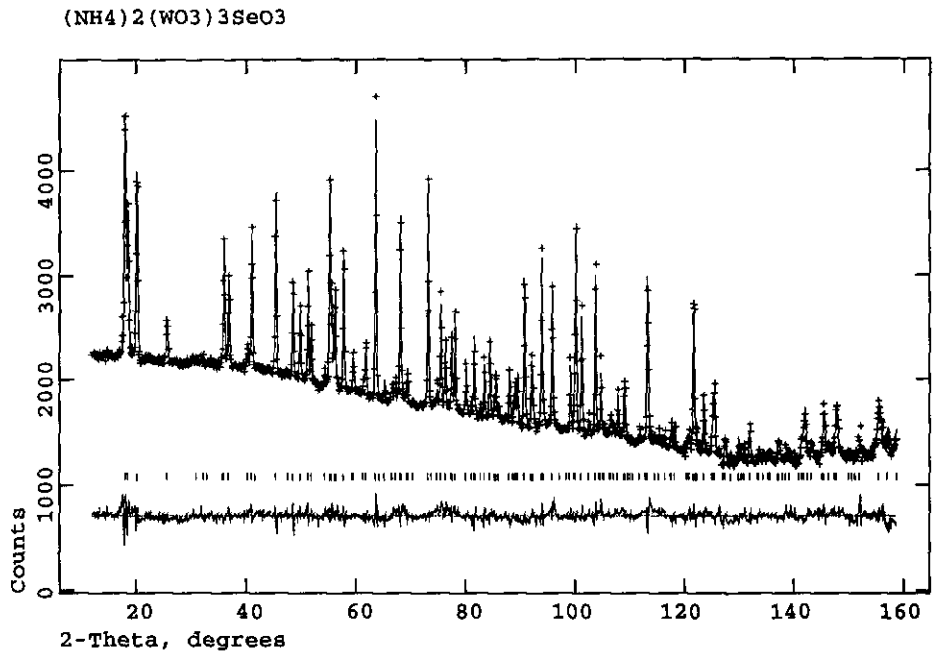

FIG. 2. Final observed (crosses), calculated (line), and difference profile plots for the Rietveld refinement of the $(NH_4)_2(WO_3)_3SeO_3$ structure. Allowed reflection positions are indicated by tick marks. Note the large incoherent background.

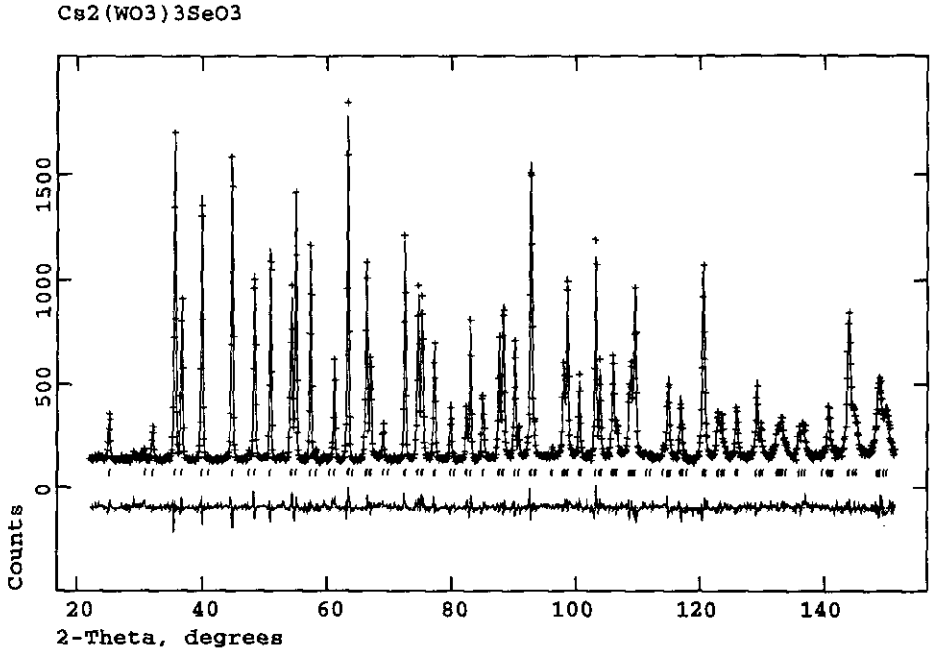

FIG. 3. Final observed (crosses), calculated (line), and difference profile plots for the Rietveld refinement of the $Cs_2(WO_3)_3SeO_3$ structure. Allowed reflection positions are indicated by tick marks.

TABLE 2
Atomic Positional/Thermal Parameters for $(NH_4)_2(WO_3)_3SeO_3$

Atom	x	y	z	U_{iso} (Å)
N(1)	1/3	2/3	0.1132(8)	0.034(3)
N(2)	1/3	2/3	−0.2669(8)	0.024(2)
W(1)	0.336(1)	0.187(2)	0.8944(6)	0.006(2)
Se(1)	0	0	0.6625(7)	0.008(2)
O(1)	0.127(2)	−0.123(2)	0.9115(8)	0.016(2)
O(2)	0.4074(8)	0.219(2)	1.0371(5)	0.013(2)
O(3)	0.543(2)	0.0847(9)	0.8507(5)	0.009(2)
O(4)	0.2449(8)	0.117(2)	0.7294(6)	0.009(2)
H(1)	0.256(5)	0.509(2)	0.1405(9)	0.0475[a]
H(2)	0.631(2)	0.184(3)	0.261(2)	0.0546[a]
H(3)	1/3	2/3	0.020(3)	0.1235[a]
H(4)	1/3	2/3	−0.350(3)	0.0724[a]

[a] $U_{eq}(Å^2) = \frac{1}{3}\sum_i\sum_j U_{ij}a_i^*a_j^*\mathbf{a}_i\cdot\mathbf{a}_j$.

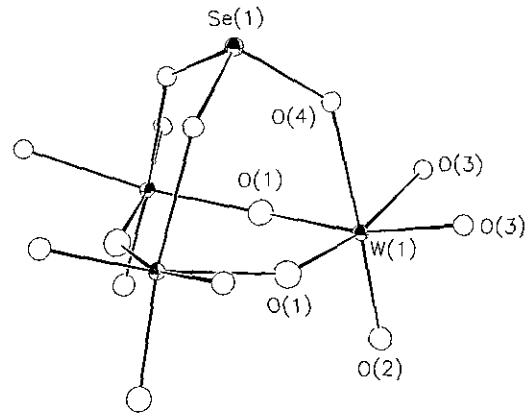

FIG. 4. ORTEP view showing detail of the W/Se/O sheet structure in $(NH_4)_2(WO_3)_3SeO_3$, showing WO_6/SeO_3 connectivity via W−O−W and W−O−Se bonds.

N(2)-centered moiety. These three O(2) atoms form a three-ring of W=O bonds on the opposite side of the $(WO_3)_3SeO_3$ layers to the capping selenium atoms. Thus, this second ammonium cation serves to "pillar" the adjacent anionic $(WO_3)_3SeO_3$ layers.

The structural motif in $(NH_4)_2(WO_3)_3SeO_3$ consists of hexagonal-tungsten-oxide like layers of vertex-sharing WO_6 octahedra in the [110] crystallographic plane. The planar connectivity of these groups results in three- and six-ring holes in the tungsten-oxygen sheet (Fig. 1). Half of the three rings are capped by Se atoms, as noted above. The W−O(1)−W′ bonds, which form the capped 3-rings, and W−O(3)−W′ bonds, which form the uncapped 3-rings, both show some degree of short–long W−O bond length "alternation" (2). The apical oxygen atoms, O(2) and O(4), project into the interplanar region of the structure. The selenium atom caps all the O(4) atoms in the structure, while the O(2) atoms are uncapped, resulting in the W(1)=O(2) bonds. All the W(1)−O(4)−Se(1) capping occurs on one side of the W/O sheet, and a very asymmetric layered structure results (Fig. 5).

TABLE 3
Bond Distances (Å) and Angles (°) for $(NH_4)_2(WO_3)_3SeO_3$

N(1)−H(1) × 3	1.04(1)	N(1)−H(3)	1.14(3)
N(2)−H(2) × 3	1.04(2)	N(2)−H(4)	1.01(4)
W(1)−O(1)	1.99(2)	W(1)−O(1)	1.82(2)
W(1)−O(2)	1.790(9)	W(1)−O(3)	2.05(2)
W(1)−O(3)	1.84(2)	W(1)−O(4)	2.091(9)
Se(1)−O(4) × 3	1.736(6)		
O(2)−H(4)[a]	2.13(3)	O(3)−H(2)[a]	2.02(2)
O(4)−H(1)[a]	1.98(2)		
H(1)−N(1)−H(1)	110.3(7)	H(1)−N(1)−H(3)	108.6(8)
H(2)−N(2)−H(4)	109.1(9)	H(2)−N(2)−H(2)	109.8(9)
O(1)−W(1)−O(1)	90.6(4)	O(1)−W(1)−O(2)	93.0(6)
O(1)−W(1)−O(3)	84.1(4)	O(1)−W(1)−O(3)	167.8(6)
O(1)−W(1)−O(4)	81.7(4)	O(1)−W(1)−O(2)	94.8(6)
O(1)−W(1)−O(3)	169.4(6)	O(1)−W(1)−O(3)	96.1(5)
O(1)−W(1)−O(4)	88.3(5)	O(2)−W(1)−O(3)	94.6(5)
O(2)−W(1)−O(3)	96.5(6)	O(2)−W(1)−O(4)	173.9(9)
O(3)−W(1)−O(3)	87.6(4)	O(3)−W(1)−O(4)	81.9(4)
O(3)−W(1)−O(4)	88.4(5)	O(4)−Se(1)−O(4)	99.9(4)
W(1)−O(1)−W(1)	146.3(4)	W(1)−O(3)−W(1)	135.2(5)
W(1)−O(4)−Se(1)	133.3(5)		

[a] H-bonding link.

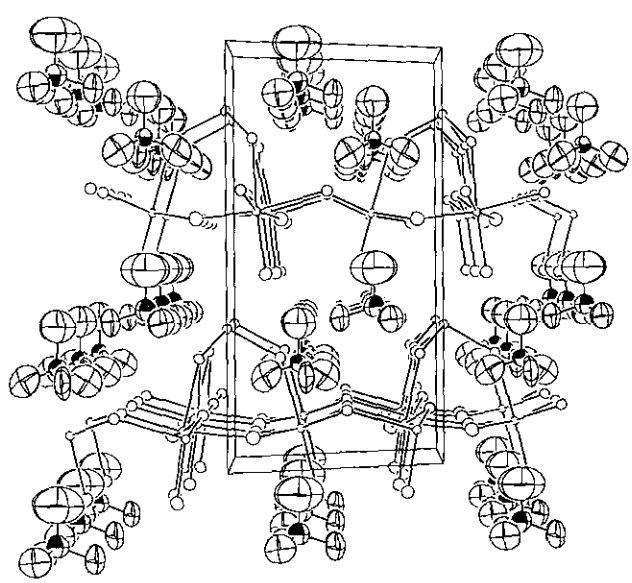

FIG. 5. The crystal structure of $(NH_4)_2(WO_3)_3SeO_3$, viewed down [010], showing the WO_6/SeO_3 sheet structure and interlayer NH_4 entities.

TABLE 4
Atomic Positional/Thermal Parameters for $Cs_2(WO_3)_3SeO_3$

Atom	x	y	z	$U_{iso}(Å^2)$
Cs(1)	1/3	2/3	0.0897(6)	0.0373[a]
Cs(2)	1/3	2/3	−0.2733(6)	0.0140[a]
W(1)	0.3376(7)	0.1483(8)	0.8968(4)	0.009(1)
Se(1)	0	0	0.6695(3)	0.0057(9)
O(1)	0.126(2)	−0.124(2)	0.9047(4)	0.0116(9)
O(2)	0.3979(6)	0.196(2)	1.0285(3)	0.0129(8)
O(3)	0.549(2)	0.0900(5)	0.8523(3)	0.0062(9)
O(4)	0.2483(5)	0.114(2)	0.7280(3)	0.009(1)

[a] $U_{eq}(Å^2) = \frac{1}{3}\sum_i\sum_j U_{ij}a_i^*a_j^*\mathbf{a}_i\cdot\mathbf{a}_j$.

The $(WO_3)_3SeO_3$ layers make an *ABAB* ... repeat motif in the crystallographic z direction. Because adjacent $(WO_3)_3SeO_3$ layers are rotated in the [110] plane with respect to one another, there are no pseudo-one-dimensional channels in this structure, comparable to the infinite [001] channels found in hexagonal-WO_3 and M_xWO_3 (M = Rb, K, NH_4 ...) type materials (4, 12).

$Cs_2(WO_3)_3SeO_3$. Structural and geometrical data for $Cs_2(WO_3)_3SeO_3$ are listed in Tables 4 and 5. $Cs_2(WO_3)_3SeO_3$ (Fig. 6) is isostructural with $(NH_4)_2(WO_3)_3SeO_3$ (Cs replacing NH_4). The octahedral W atom in $Cs_2(WO_3)_3SeO_3$ is displaced 0.27 Å from the geometrical center of its six O atom neighbors (see Fig. 7) and as with the $(NH_4)_2(WO_3)_3SeO_3$ structure, this distortion is locally toward an octahedral face. The BVS of tungsten is 6.33, in reasonable accord with the 6.00 expected for W^{VI}.

TABLE 5
Bond Distances (Å)/Angles (°) for $Cs_2(WO_3)_3SeO_3$

Cs(1)−O(1) × 3	3.496(8)	Cs(1)−O(4) × 3	3.152(6)
Cs(2)−O(1) × 3	3.438(7)	Cs(2)−O(2) × 3	3.006(8)
Cs(2)−O(3) × 3	3.093(5)		
W(1)−O(1)	1.80(2)	W(1)−O(1)	2.03(1)
W(1)−O(2)	1.700(6)	W(1)−O(3)	1.87(1)
W(1)−O(3)	2.02(1)	W(1)−O(4)	2.192(5)
Se(1)−O(4) × 3	1.727(4)		
O(1)−W(1)−O(1)	90.8(3)	O(1)−W(1)−O(2)	99.3(4)
O(1)−W(1)−O(3)	96.4(3)	O(1)−W(1)−O(3)	165.6(4)
O(1)−W(1)−O(4)	83.5(4)	O(1)−W(1)−O(2)	92.5(4)
O(1)−W(1)−O(3)	164.0(4)	O(1)−W(1)−O(3)	83.7(3)
O(1)−W(1)−O(4)	81.5(4)	O(2)−W(1)−O(3)	100.3(5)
O(2)−W(1)−O(3)	94.2(4)	O(2)−W(1)−O(4)	173.5(5)
O(3)−W(1)−O(3)	85.9(3)	O(3)−W(1)−O(4)	85.2(4)
O(3)−W(1)−O(4)	82.6(4)	O(4)−Se(1)−O(4)	103.3(2)
W(1)−O(1)−W(1)	148.5(3)	W(1)−O(3)−W(1)	135.0(3)
W(1)−O(4)−Se(1)	130.1(3)		

The two cesium cations in $Cs_2(WO_3)_3SeO_3$ occupy special positions in the interlayer region, both with three-fold site symmetry. Cs(1) and Cs(2) sites alternate in the z direction, but their coordinations are different: Cs(1) [equivalent to the N(1)H_4 cation in $(NH_4)_2(WO_3)_3SeO_3$] makes six bonds to nearby oxygen atoms (Fig. 8) in distorted trigonal prismatic coordination. Cs(2) bonds to nine nearby O atoms (six below and three above); the six lower oxygen atoms associated with an octahedral six-ring form a chair-like configuration (Fig. 9). Thus, both Cs(1) and Cs(2) make bonds to oxygen atoms in the two $(WO_3)_3SeO_3$ layers adjacent to themselves, compared to the situation in the $(NH_4)_2(WO_3)_3SeO_3$ where only one of the two distinct ammonium cation makes trans-layer connections. Neither of the BVS values for the cesium cations in $Cs_2(WO_3)_3SeO_3$ (BVS[Cs(1)] = 0.57; BVS[Cs(2)] = 1.29) is especially close to the expected value of 1.00 for Cs^+. This suggests that the stability of this structure type is not crucially determined by the bonding requirements of the guest cations. However, these species must have some role to play in stabilizing the HTO-type six-ring windows, and must be large enough to bridge adjacent $(WO_3)_3SeO_3$ layers. We are doing further work to elucidate the stability limits of this structure with respect to cation size.

Thermogravimetric analysis for $(NH_4)_2(WO_3)_3SeO_3$ showed a two-step weight loss at ~350 and 450°C. An overall weight loss of 18.9% correlates well with the expected weight loss of 19.0% for complete nominal elimination of H_2O, NH_3, and SeO_2 from $(NH_4)_2(WO_3)_3SeO_3$, leaving a residue of tungsten trioxide. The 500°C residue (nitrogen atmosphere) consisted of hexagonal WO_3 (4, 13). Further heating to 600°C under nitrogen converted this metastable phase to triclinic WO_3 (14). Conversely, a TGA run carried out under flowing oxygen resulted in a mixture of hex-WO_3 and triclinic WO_3 at 500°C.

TGA showed that the $Cs_2(WO_3)_3SeO_3$ sample lost 10.4% of its weight in one step between 500 and 600°C. The expected weight loss for sublimation of all the selenium (as SeO_2) in this compound is 10.2%. The off-white post-TGA residue consists of $Cs_2W_3O_{10}$, of unknown structure (15).

The infrared spectrum of $(NH_4)_2(WO_3)_3SeO_3$ is shown in Fig. 10. Two prominent regions associated with NH_4^+ vibrations may be identified. Three bands at 3160, 3019, and 2810 cm^{-1} represent symmetric ν_1 and asymmetric ν_3 NH_4^+ stretches for the two distinct NH_4^+ species. The two bands at 1468 and 1414 cm^{-1} correlate with the ν_4 asymmetric stretching modes for the two distinct ammonium cations in this compound. These bands are similar to those reported earlier for the IR spectrum of $(NH_4)_2(MoO_3)_3SeO_3$ (2). A sharp band at 960 cm^{-1} is a bound Se−O (selenite) stretching mode (2), while the complex, overlapping group of bands in the region 790–640 cm^{-1} correspond to unresolved modes for the WO_6 and SeO_3 groups.

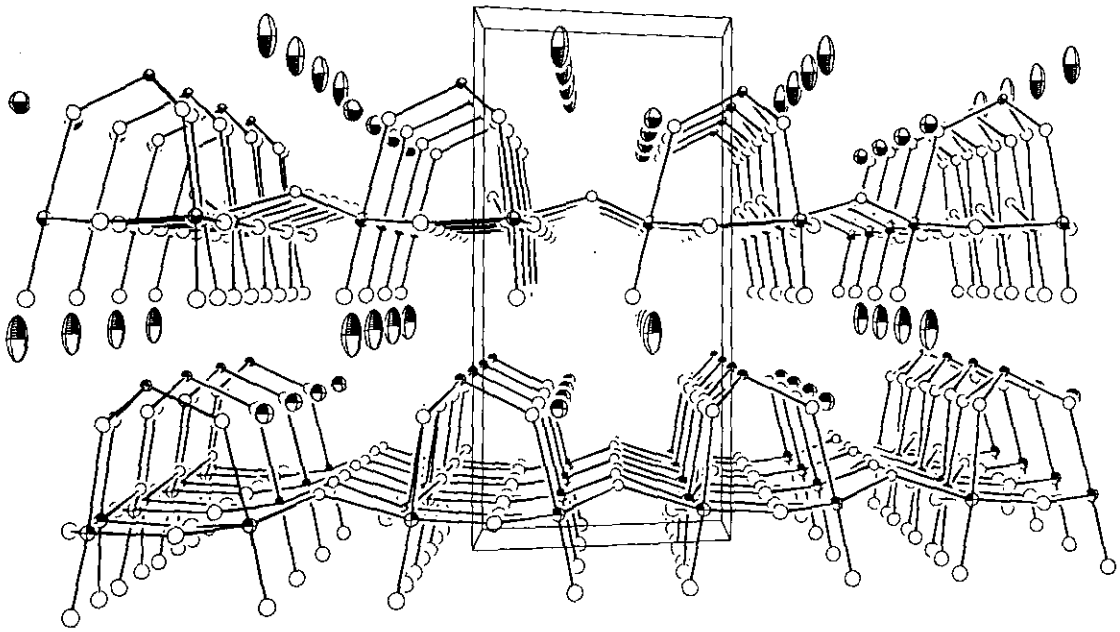

FIG. 6. The $Cs_2(WO_3)_3SeO_3$ crystal structure, viewed down [010].

As expected, the infrared spectrum of $Cs_2(WO_3)_3SeO_3$ (Fig. 11) is featureless between 4000 and 1200 cm^{-1}. A sharp band at 947 cm^{-1} corresponds to the selenite mode noted above for $(NH_4)_2(WO_3)_3SeO_3$. We ascribe the broad, overlapping features in the region 800–600 cm^{-1} to various unresolved Se/O and W/O modes.

The Raman spectrum of $Cs_2(WO_3)_3SeO_3$ is shown in Fig. 12. Peaks below ~300 cm^{-1} correspond to lattice (phonon) modes in this phase (16). The strong, broad peak at 638 cm^{-1} is associated with a symmetric stretching mode for the WO_6 entity (corresponding IR peak seen at 640 cm^{-1}). Raman peaks at 598, 678, and 706 cm^{-1} are also associated with WO_6 modes. A peak at 804 cm^{-1} corresponds to the symmetric stretching mode of the pyramidal SeO_3 group, as seen in related layered selenite phases (1, 2).

CONCLUSIONS

$(NH_4)_2(WO_3)_3SeO_3$ and $Cs_2(WO_3)_3SeO_3$ have been prepared and characterized for the first time. They are isostructural phases based on a single layer of the hexagonal

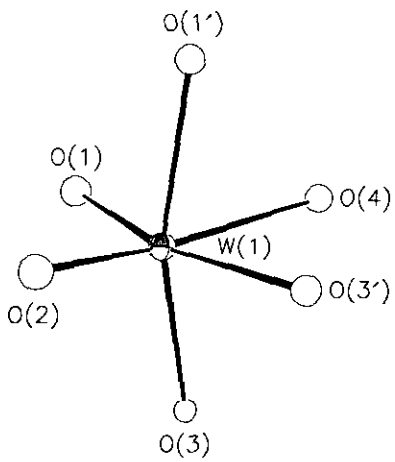

FIG. 7. Tungsten coordination in $Cs_2(WO_3)_3SeO_3$, showing displacement of the W atom from the center of the WO_6 octahedron toward the octahedral face defined by atoms O(1), O(2), and O(3).

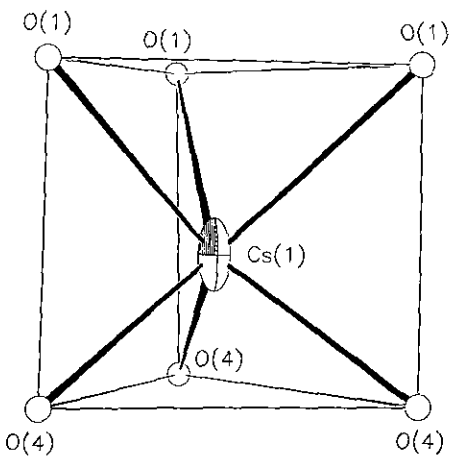

FIG. 8. Sixfold Cs(1) coordination to oxygen in the $Cs_2(WO_3)_3SeO_3$ structure.

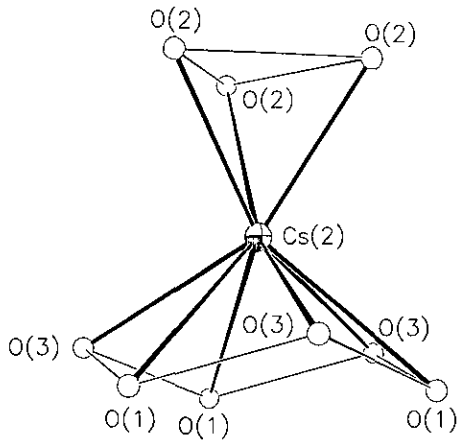

FIG. 9. Ninefold Cs(2) coordination to oxygen in the $Cs_2(WO_3)_3SeO_3$ structure.

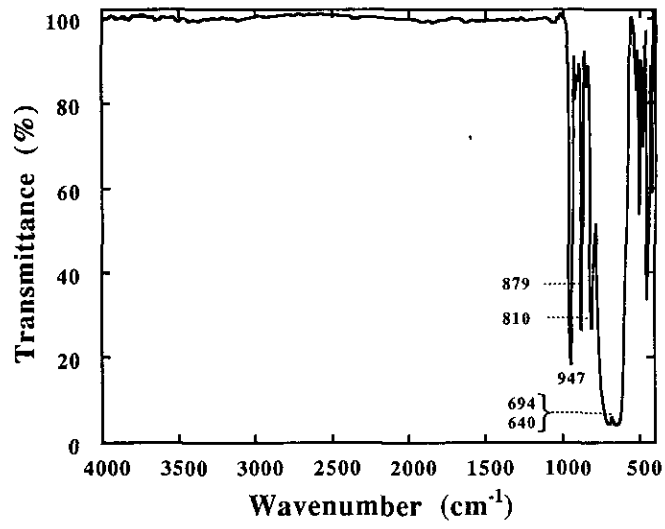

FIG. 11. Infrared spectrum of $Cs_2(WO_3)_3SeO_3$.

tungsten oxide motif of corner-sharing WO_6 octahedra. Selenium(IV) atoms (as part of $[SeO_3]^{2-}$ selenite groups) cap one side of the W/O sheets, and ammonium or cesium cations provide interlayer charge balancing. Powder neutron diffraction was successful in elucidating the hydrogen atom positions in $(NH_4)_2(WO_3)_3SeO_3$, allowing the H-bonding configuration to be determined for this protonic material. Because of the staggered stacking arrangement of the $(WO_3)_3SeO_3$ sheets, there are no pseudo-infinite channels in these structures comparable to those found in hex-WO_3.

$(NH_4)_2(WO_3)_3SeO_3$ and $Cs_2(WO_3)_3SeO_3$ are isostructural with their molybdenum(VI)-containing analogues $(NH_4)_2(MoO_3)_3SeO_3$ and $Cs_2(MoO_3)_3SeO_3$ (2). There are notable similarities in the detailed octahedral-metal coordinations: Both tungsten and molybdenum show a distinctive displacement toward an octahedral face inside their oxygen atom octahedra, although the magnitude of the Mo atom displacement (0.33 Å for $(NH_4)_2(MoO_3)_3SeO_3$; 0.30 Å for $Cs_2(MoO_3)_3SeO_3$) is somewhat larger than that observed for the W atoms in $(NH_4)_2(WO_3)_3SeO_3$ (0.20 Å) and $Cs_2(WO_3)_3SeO_3$ (0.27 Å). The smaller distortion (off-center displacement of the W atoms) in the tungsten compounds is consistent with the general observation that distortions around d^0 transition metals increase with increasing cation charge, but *decrease* with increasing cation size (17). However, such distortions from octahedral regularity are not always observed for related phases containing

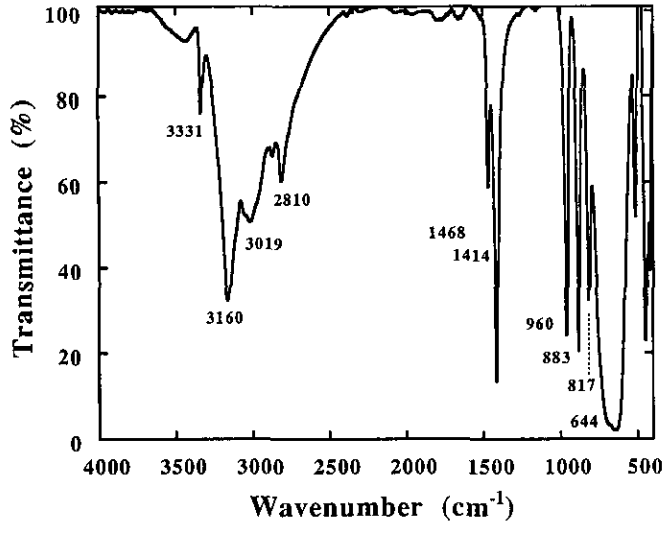

FIG. 10. Infrared spectrum of $(NH_4)_2(WO_3)_3SeO_3$.

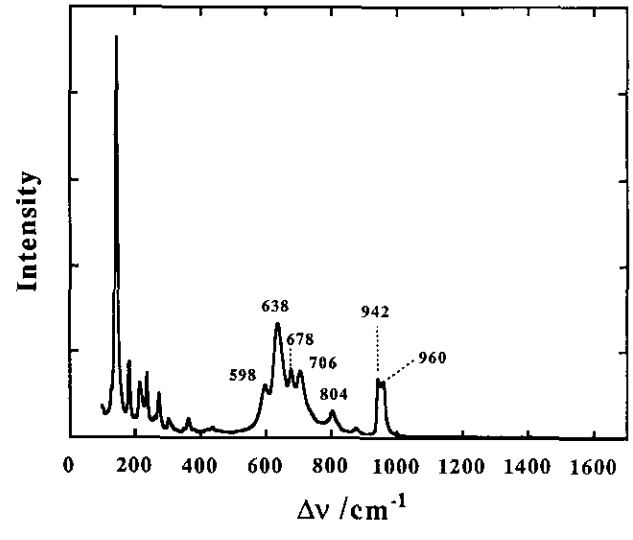

FIG. 12. Raman spectrum of $Cs_2(WO_3)_3SeO_3$.

tungsten(VI): In hex-WO_3 itself, the WO_6 octahedron is almost regular, and the W atom occupies a center of symmetry (4).

ACKNOWLEDGMENTS

We thank the National Science Foundation (DMR9214804) and the R. A. Welch Foundation for partial financial support. The neutron diffraction experiments are supported by the Division of Materials Sciences, U.S. Department of Energy, under Contract DEA-AC02-76CH00016.

REFERENCES

1. J. T. Vaughey, W. T. A. Harrison, L. L. Dussack, and A. J. Jacobson, *Inorg. Chem.* **33,** 4370 (1994).
2. W. T. A. Harrison, L. L. Dussack, and A. J. Jacobson, *Inorg. Chem.* **33,** 6043 (1994).
3. W. T. A. Harrison, L. L. Dussack, and A. J. Jacobson, *Inorg. Chem.*, in press (1995).
4. B. Gérand, G. Nowogrocki, J. Guenot, and M. Figlarz, *J. Solid State Chem.* **29,** 429 (1979).
5. W. T. A. Harrison, L. L. Dussack, and A. J. Jacobson, *Acta Crystallogr.*, in press (1995).
6. A. Le Bail, G. Férey, P. Amoros, and D. Beltran-Porter, *Eur. J. Solid State Inorg. Chem.* **26,** 419 (1989).
7. W. T. A. Harrison, A. V. P. McManus, M. P. Kaminsky and A. K. Cheetham, *Chem. Mater.* **5,** 1631 (1993).
8. A. C. Larson and R. B. Von Dreele, "GSAS User Guide." Los Alamos National Laboratory, Los Alamos, New Mexico, 1995.
9. P. Thompson, D. E. Cox, and J. B. Hastings, *J. Appl. Crystallogr.* **20,** 79 (1987).
10. N. E. Brese and M. O'Keeffe, *Acta Crystallogr. Sect. B* **47,** 192 (1991).
11. R. E. Morris, W. T. A. Harrison, G. D. Stucky, and A. K. Cheetham, *J. Solid State Chem.* **94,** 227 (1991).
12. P. H. Labbe, M. Goreaud, B. Raveau, and J. C. Monier, *Acta Crystallogr. Sect. B* **34,** 1433, (1978).
13. JCPDS Powder Diffraction File, Card No. 33-1387.
14. JCPDS Powder Diffraction File, Card No. 32-1395.
15. E. M. Novikova and A. A. Maier, *Inorg. Mater. USSR* **8,** 1421 (1972).
16. K. Nakamoto, "Infrared and Raman Spectra of Inorganic and Coordination Compounds," 9th ed. Wiley–Interscience, New York, 1986.
17. M. Kunz and I. D. Brown, *J. Solid State Chem.* **115,** 395 (1995).